Frequency-Modulated Chirp Signals for Single-Photodiode Based Coherent LiDAR System

Wenting Yi ⓘ, *Student Member, IEEE*, Zhe Li ⓘ, *Member, IEEE*, Zichuan Zhou ⓘ, *Student Member, IEEE*, Eric Sillekens ⓘ, *Member, IEEE*, Thomas Gerard ⓘ, *Student Member, IEEE*, Callum Deakin ⓘ, *Student Member, IEEE*, Filipe M. Ferreira ⓘ, *Senior Member, IEEE*, Lidia Galdino ⓘ, *Member, IEEE*, Zhixin Liu ⓘ, *Senior Member, IEEE*, Polina Bayvel ⓘ, *Fellow, IEEE*, and Robert I. Killey ⓘ, *Senior Member, IEEE*

Abstract—In this paper, we investigate two categories of linear frequency-modulated chirp signals suitable for single-photodiode based coherent light detection and ranging (LiDAR) systems, namely, the frequency-modulated continuous-wave (FMCW) single-sideband (SSB) signal and the amplitude-modulated double-sideband (DSB) signal, and compare their achievable receiver sensitivity performance. The DSB signal requires a simpler transmitter design, as it is real-valued and can be generated using a single-drive Mach-Zehnder modulator (MZM), while the SSB signal, which is frequency/phase modulated, requires an in-phase and quadrature modulator (IQM)-based transmitter. A theoretical analysis of direct-detection (DD) beating interference (BI) especially the local oscillator (LO) beating with itself, known as LO-LO BI, is presented. Both Monte Carlo simulations and experimental demonstrations are carried out. Good agreement between simulations and experiments is achieved. In comparison with the SSB system, the DSB signal-based system is affected by laser phase noise-induced power fluctuation, and also suffers a significant sensitivity penalty due to nonlinear LO-LO BI. A spectral guard band for mitigating LO-LO BI is necessary for the DSB signal, achieved at the expense of requiring a larger electrical bandwidth. In system tests with a delay line of 385 m, the SSB signal outperforms the DSB signal with a 10 dB better receiver sensitivity in the case with a guard band, and 25 dB better sensitivity without a guard band.

Index Terms—Coherent detection, frequency-modulated continuous-wave, light detection and ranging.

I. INTRODUCTION

LIGHT detection and ranging (LiDAR) systems have been widely studied for numerous applications such as autonomous vehicles, 3D imaging and anemometry [1]–[6]. Pulsed

Wenting Yi, Zichuan Zhou, Eric Sillekens, Thomas Gerard, Callum Deakin, Filipe M. Ferreira, Lidia Galdino, Zhixin Liu, Polina Bayvel, and Robert I. Killey are with Optical Networks Group, Department of Electronic and Electrical Engineering, University College London, WC1E 7JE London, U.K. (e-mail: w.yi.17@ucl.ac.uk; zichuan.zhou.14@ucl.ac.uk; e.sillekens@ucl.ac.uk; thomas.gerard.15@ucl.ac.uk; callum.deakin.17@ucl.ac.uk; filipef@ieee.org; l.galdino@ucl.ac.uk; zhixin.liu@ucl.ac.uk; p.bayvel@ucl.ac.uk; r.killey@ucl.ac.uk).

Zhe Li is with Finisar Corporation, Sunnyvale, CA 94089 USA (e-mail: zhe.li@ieee.org).

direct-detection (DD) LiDAR is one of the most commonly used LiDAR architectures where the target distance is estimated from the time-of-flight of the lightwave to the target. In order to detect long-distance targets, a short pulse with a high instantaneous output power is desired while the average power should be maintained below the eye safety requirement [7], [8]. Another type of LiDAR architecture which has been gaining more research interest recently is the coherent frequency-modulated (FM) chirp LiDAR system, particularly the frequency-modulated continuous-wave (FMCW) LiDAR [9]–[12]. The mixing between a reflected chirp signal and a reference signal converts time/distance detection into a beat frequency detection. The main advantage of FM chirp LiDAR systems over pulsed LiDAR is the high ranging resolution due to the utilization of wide frequency modulation bandwidth. In addition, thanks to the coherent detection scheme, the FM chirp LiDAR system is more tolerant to ambient interference and offers a better receiver sensitivity [8], [13].

The simplest approach to generate such linear FM chirp signals is to directly modulate a laser [14], [15]. Nevertheless, due to the inherent nonlinear relation between the output frequency and the driving waveform of the tunable laser, a linearization technique is often required to optimize the signal waveform [16]–[18]. Frequency modulation of the laser by varying the injection current into the gain section also comes with an unwanted intensity modulation. To avoid this, multi-section tunable lasers can be used, which offer a wide frequency tuning range, and thus potentially a high resolution. However, they usually suffer from a larger laser phase noise, limiting the maximum operation range of the LiDAR system [19], [20]. It should be noted that it has recently been demonstrated in the literature that it is possible to implement low linewidth tunable lasers, for example, hybrid silicon photonic tunable lasers with 15 kHz linewidth [21], [22]; however, more investigations on their tuning speed are necessary, as this is also critical for a LiDAR source.

An alternative method to generate the chirp signal is to use a continuous wave (CW) laser followed by an external electro-optical modulator (EOM). Though this approach adds complexity to the system setup, it offers several advantages over using tunable lasers. First, it allows to use a narrow-linewidth laser of conventional design (e.g., an external cavity laser (ECL)), providing a longer coherence length and LiDAR operation distance. Besides, a better modulation linearity and control of the
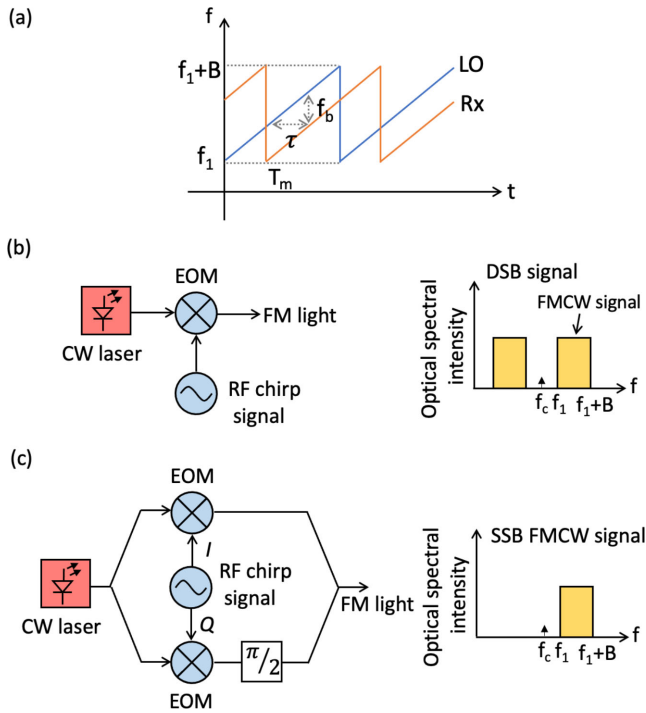
Fig. 1. (a) Instantaneous frequency versus time of a time-delayed received sawtooth chirp waveform and its local reference in a coherent LiDAR system; Block diagram of linear FM signal generation by: (b) EOM for DSB signal; (c) IQM for SSB FMCW signal. LO: local oscillator; Rx: received signal; CW: continuous wave; EOM: electro-optical modulator; RF: radio frequency; FM: frequency-modulated; I: in-phase; Q: quadrature; DSB: double-sideband; SSB: single-sideband; FMCW: frequency-modulated continuous-wave [19].

frequency and amplitude of the optical signal waveform can be achieved via external modulators.

Two types of external EOMs are commonly used. To generate the FMCW chirp signal which is frequency/phase-modulated and complex-valued, an in-phase and quadrature modulator (IQM) is needed to independently modulate the in-phase and quadrature components of its incoming light [23]. The corresponding optical waveform has a constant intensity in the time domain, and a single sideband (SSB) in the frequency-domain, which can be loaded onto either side of the optical carrier. In contrast to the SSB FMCW signal, an alternative approach makes use of an amplitude modulator, such as a single-drive Mach-Zehnder modulator (MZM) to generate an amplitude-modulated and real-valued FM chirp signal [8], [24]. In the frequency-domain, this is a double-sideband (DSB) signal in which each sideband, when considered separately, is an FMCW waveform, and the lower sideband is simply the complex conjugate of the upper sideband (see Fig. 1). Although this chirp signal is amplitude-modulated, the operating principle of the DSB system is very similar to that of the SSB FMCW system, and it has been successfully demonstrated for range and velocity estimation with a balanced phase-diversity coherent receiver [8], [24]. The single-drive MZM used in the DSB system is simpler than the IQM required for SSB signal generation.

To achieve coherent detection at the receiver, the local oscillator (LO) can either be a CW laser [25], [26] or an FM chirp signal [8], [24]. In the case of a CW laser, the LO's role

is to amplify the received signal (Rx) and down-convert the signal to the baseband. The detected photocurrent is a delayed chirp and an electrical mixer is required for de-chirping [23], [26]. However, in this case, additional noise and nonlinearity are induced during frequency mixing and lead to degraded receiver sensitivity [8]. Alternatively, one can use an optical splitter to obtain two copies of the modulated chirp signal, transmitting one and using the other as the LO [8], [27]. The desired beat signal is produced when the LO beats with the reflected signal in photodetection. The beat frequency is used to determine the time-of-flight of the LiDAR signal. This approach relaxes the bandwidth requirement for the photodiode as the beat frequency is smaller than the chirping bandwidth. Additionally, an electrical mixer is no longer required and the receiver configuration can be greatly simplified. For this type of coherent detection scheme, it is possible to use a 3-dB coupler to combine signal and LO, with either a single-ended photodiode (PD) [16], or balanced detectors [20]. Alternatively, a balanced phase-diversity coherent receiver based on an optical 90° hybrid can be employed [24]. The combination of an IQM and a balanced phase-diversity coherent receiver offers good performance, as advanced complex signal waveforms can be designed for improving the distance and velocity estimation accuracy [25], [28]; however, the high cost and complexity of this receiver architecture remain the main concern for practical implementation. With 3-dB coupler-based balanced detection, a precise 50/50 split of the coupler and two balanced photodiodes are required in order to maximise the common mode rejection ratio (CMRR) and to completely eliminate the DD beating interference (BI). The 3-dB coupler-based receiver employing a single-ended photodiode offers the advantages of simplicity and low cost. However, the receiver sensitivity in such a receiver configuration is limited by unwanted DD beating distortions especially the LO-LO beating interference (LO-LO BI). This can be mitigated by including a sufficiently wide spectral guard band, to separate the desired signal from the DD distortions, achieved at the expense of requiring larger electrical bandwidth.

In this work, through both Monte Carlo simulations and experimental demonstrations, we investigate a low-cost and low-complexity coherent LiDAR receiver with single-photodiode detection in which the LO is a frequency-modulated chirp signal, and compare the receiver sensitivity performance difference between two chirp waveforms: 1) the frequency-modulated complex-valued SSB signal, and 2) the amplitude-modulated real-valued DSB signal. Though the DSB signal has previously been demonstrated in a balanced phase-diversity coherent LiDAR system [8], [24], its performance with a single-photodiode based coherent receiver has not been investigated before to the best of our knowledge. We analyze the direct detection beating interference arising from single-ended photodetection in the coherent receiver, and show that while the LO-LO BI for the SSB signal is just a DC component which can be easily filtered out, the DSB signal suffers a significant receiver sensitivity penalty from nonlinear LO-LO BI and requires a sufficiently wide spectral guard band for mitigation. In addition, the DSB signal is susceptible to laser phase noise as it is converted to amplitude noise after square-law detection on reception, leading to a power

fluctuation of the desired beat frequency. Both simulation and experimental results indicate that with a delay line of 385 m, when LO-LO BI is mitigated through the use of a guard band, the SSB FMCW signal offers 10 dB better receiver sensitivity than the DSB signal. Without the use of a guard band, the advantage of the SSB signal increases to 25 dB. Furthermore, at a shorter delay distance of 44 m, the SSB signal is shown to outperform the DSB signal, with 25 dB better sensitivity even when the LO-LO BI is mitigated using a guard band for the DSB signal. Note that in [8], [24], the LO-LO BI associated with the DSB signal is suppressed through balanced detection. However, as mentioned earlier, ideal mitigation of LO-LO BI requires a high common mode rejection ratio, otherwise residual LO-LO BI will remain which may still cause sensitivity penalty when using a DSB signal.

The rest of the paper is organized as follows: in Section II, we discuss the modulation scheme of SSB and DSB signals. We mathematically analyze the desired beat frequency and the beating interference in the coherent single-photodiode receiver. Section III describes the system setup for both simulations and experiments, followed by a discussion of results in Section IV. Section V concludes the paper.

II. THEORY

A. Signal Modulation

For a typical sawtooth chirp as shown in Fig. 1(a), the frequency changes linearly with time, expressed as:

$$\cos(\varphi(t)) = \cos\left(2\pi f_1 t + \frac{\pi B t^2}{T_m}\right) \quad (1)$$

where f_1 denotes the lower boundary of the chirp signal (the frequency range from 0 Hz to f_1 is referred to as the guard band), t is the time instance, B represents the chirping bandwidth and T_m is the chirp repetition period.

Fig. 1(b) shows the block diagram of the transmitter for the DSB signal, comprising a CW laser followed by an external EOM, (for example a single-drive MZM), to generate an amplitude-modulated FM chirp [8], [24]. The signal has two modulation sidebands centered on the optical carrier frequency of f_c. Biasing the modulator at the minimum transmission, the optical carrier can be suppressed. To generate such a signal, the driving voltage $V(t)$ of the MZM is described as:

$$V(t) = V_D \cos(\varphi(t)) = V_D \cos\left(2\pi f_1 t + \frac{\pi B t^2}{T_m}\right) \quad (2)$$

where V_D is the amplitude of the driving voltage. The transfer function of a MZM is given by [29]:

$$E_{\text{out}}(t) = E_{\text{in}}(t) \cos\left(\frac{\phi(t)}{2} + \phi_0\right), \quad \phi(t) = \frac{\pi V(t)}{V_\pi} \quad (3)$$

where $E_{\text{in}}(t)$ and $E_{\text{out}}(t)$ are the input and output electrical fields of the light, ϕ_0 is the initial phase related to the direct current (DC) bias. The phase shift $\phi(t)$ is proportional to the driving voltage $V(t)$. V_π denotes a driving voltage which produces a π phase shift between two arms of an MZM (i.e., $\phi(V_\pi) = \pi$).

Substituting Eq. 2 into Eq. 3, assuming the MZM modulation is linear (i.e., $\frac{V_D}{V_\pi} \ll 1$) and biased at the minimum transmission point ($\phi_0 = -\frac{\pi}{2}$), the output of the MZM is:

$$E_{\text{out}}(t) = E_{\text{in}}(t) \cos\left(\frac{\pi V_D}{2V_\pi} \cos(\varphi(t)) - \frac{\pi}{2}\right)$$

$$\approx E_{\text{in}}(t) \cos(\varphi(t)) \quad (4)$$

Eq. 4 represents the double-sided sawtooth waveform with carrier suppressed. If the incoming optical light $E_{\text{in}}(t)$ of the MZM is corrupted by laser phase noise, then Eq. 4 can be written as:

$$E_{\text{out}}(t) = E_{\text{in}}(t) \cos(\varphi(t)) = A \cos(\varphi(t)) e^{j(\omega_c t + \theta(t))} \quad (5)$$

where A and ω_c denote the amplitude and the angular carrier frequency ($\omega_c = 2\pi f_c$) of the laser source, $\theta(t)$ is the laser phase noise.

In contrast to the DSB signal which is real-valued and amplitude-modulated, the complex SSB FMCW signal, as shown in Fig. 1(c), can be generated using an IQM by independently modulating the in-phase and quadrature components [19], [23]. The SSB signal has a constant intensity with one modulation sideband. The real and imaginary parts of a SSB signal are related to each other by the Hilbert transform. The corresponding driving voltages of the IQM are defined as:

$$V_I(t) = V_D \cos(\varphi(t)), \quad V_Q(t) = V_D \sin(\varphi(t)) \quad (6)$$

The transfer function of an IQM is given by [29]:

$$E_{\text{out}}(t) = \frac{1}{2} E_{\text{in}}(t) \left(\cos\left(\frac{\phi_I(t)}{2}\right) + j \cos\left(\frac{\phi_Q(t)}{2}\right)\right) \quad (7)$$

where $\phi_I(t) = \frac{\pi V_I(t)}{V_\pi}$ and $\phi_Q(t) = \frac{\pi V_Q(t)}{V_\pi}$, j denotes the $\frac{\pi}{2}$ phase shift induced on the light passing through one of the two EOMs in the IQM and the factor of $\frac{1}{2}$ indicates the 50/50 splitting ratio.

Similarly to the case with the DSB signal, the IQM is assumed to be biased at the null point and to operate in the linear region. Combining Eq. 6 and Eq. 7, the generated SSB FMCW signal at the output of IQM is:

$$E_{\text{out}}(t) = \frac{1}{2} E_{\text{in}}(t)(\cos(\varphi(t)) + j \sin(\varphi(t)))$$

$$= \frac{1}{2} A e^{j(\omega_c t + \varphi(t) + \theta(t))} \quad (8)$$

B. Beating Products

In the single-photodiode-based coherent receiver with LO as a chirp signal, the LO and the out-going signal are usually split after amplification at the transmitter, for example by an Erbium-doped fiber amplifier (EDFA) [24], [30]. In this case, both the transmitted signal and LO are corrupted by amplified spontaneous emission (ASE) noise. At the receiver, a 3-dB coupler is used to combine the LO and the Rx signal which is time-delayed by τ accounting for the round-trip delay (see Fig. 1(a)). The optical field at the output of the coupler is:

$$E = \frac{1}{\sqrt{2}} \left[E_{\text{LO}} + E_{\text{ASE(LO)}} + j(E_{\text{Rx}} + E_{\text{ASE(Rx)}})\right] \quad (9)$$

where E_{LO} and E_{Rx} represent the ASE-noise-free LO and Rx signal, $E_{\text{ASE(LO)}}$ and $E_{\text{ASE(Rx)}}$ denote the ASE noise from the LO and Rx signal. Following single-photodiode square-law detection, the photocurrent is given by:

$$I_{\text{PD}} \propto \text{R}|E|^2$$

$$\propto \frac{\text{R}}{2} \left(\underbrace{|E_{\text{LO}}|^2}_{\text{LO-LO beating}} + |E_{\text{Rx}}|^2 + |E_{\text{ASE(LO)}}|^2 + |E_{\text{ASE(Rx)}}|^2 \right.$$

$$+ \underbrace{2\Re\left[E_{\text{LO}}E^*_{\text{ASE(LO)}}\right]}_{\text{LO-ASE beating}} + 2\Re\left[E_{\text{Rx}}E^*_{\text{ASE(Rx)}}\right]$$

$$+ \underbrace{2\Im\left[E_{\text{Rx}}E^*_{\text{LO}}\right]}_{\text{LO-signal beating}} + 2\Im\left[E_{\text{ASE(Rx)}}E^*_{\text{LO}}\right]$$

$$\left. + 2\Im\left[E_{\text{ASE(Rx)}}E^*_{\text{ASE(LO)}}\right] + 2\Im\left[E_{\text{Rx}}E^*_{\text{ASE(LO)}}\right] \right)$$

$$(10)$$

where R is the responsivity of the PD, the asterisk denotes complex conjugation, and $\Re[x]$ and $\Im[x]$ represent the real and imaginary parts of x. In Eq. 10, LO-signal beating is the desired beating term which produces the desired beat frequency. All the other beating products are unwanted impairments which will degrade the receiver sensitivity. In particular, as the LO is very strong, the LO-ASE beating interference (LO-ASE BI, broadband white noise) and LO-LO BI (related to the LO waveform) will fundamentally limit the receiver sensitivity.

In the case of the amplitude-modulated DSB signal, the desired LO-signal beating product can be written as:

$$I^{\text{DSB}}_{\text{LO-signal}} \propto \text{R}\Im\left[E_{\text{Rx}}E^*_{\text{LO}}\right]$$

$$\propto \text{R}A_{\text{Rx}}A_{\text{LO}}\cos(\varphi(t-\tau))\cos(\varphi(t))\sin(\Delta\theta(t))$$

$$\propto \frac{1}{2}\text{R}A_{\text{Rx}}A_{\text{LO}}\sin(\Delta\theta(t))$$

$$\times \left[\cos(\Delta\varphi(t)) + \cos(\varphi(t-\tau) + \varphi(t))\right] \quad (11)$$

where A_{LO} and A_{Rx} denote the amplitude of the LO and Rx signal, τ is the round-trip delay, and $\cos(\Delta\varphi(t))$ denotes the desired component at the beat frequency which is the frequency offset between the LO and the reflected Rx signal. $\cos(\varphi(t-\tau)+\varphi(t))$ is a beating image and it corresponds to the sum of the frequencies of the LO and Rx signal. $\Delta\theta(t)$ refers to the variation of the laser phase noise between the LO and Rx signal. It is converted into amplitude noise after photodetection, introducing a power fluctuation to the desired beat signal. The LO-LO beating interference when using the DSB signal is:

$$I^{\text{DSB}}_{\text{LO-LO BI}} \propto \frac{\text{R}}{2}|E_{\text{LO}}|^2$$

$$\propto \frac{\text{R}}{2}|A_{\text{LO}}\cos(\varphi(t))|^2$$

$$\propto \frac{1}{4}\text{R}A^2_{\text{LO}}(1 + \cos(2\varphi(t))) \quad (12)$$

It can be seen that for a DSB signal, the LO-LO BI manifests as a constant DC term plus a nonlinear beating interference starting at a frequency of $2f_1$ with twice the bandwidth of the chirp signal. While the DC component can be easily filtered out using a DC blocker, the nonlinear interference will distort any desired LO-signal beating products which fall within the same frequency range. Therefore, a spectral guard band would be necessary to separate the desired beating products from the LO-LO BI. For a sawtooth waveform as considered in this work, the maximum possible delay is equal to half of the pulse period, leading to a maximum beat frequency f_b of $\frac{B}{2}$. Hence, a minimum guard band of $\frac{B}{4}$ is necessary in order to mitigate LO-LO BI (i.e., $f_1 > \frac{B}{4}$).

In contrast, for a SSB FMCW signal, the desired LO-signal beating product is:

$$I^{\text{SSB}}_{\text{LO-signal}} \propto \text{R}\Im\left[E_{\text{Rx}}E^*_{\text{LO}}\right]$$

$$\propto \text{R}\Im\left(A_{\text{Rx}}A_{\text{LO}}e^{j(\Delta\varphi(t)+\Delta\theta(t))}\right)$$

$$\propto \text{R}A_{\text{Rx}}A_{\text{LO}}\sin(\Delta\varphi(t)+\Delta\theta(t)) \quad (13)$$

After photodetection, the phase noise variation $\Delta\theta(t)$ is added to the desired beat frequency. However, as long as the round-trip-distance is within the laser coherence length, the variation of the phase noise between the LO and Rx signal will be negligible (i.e., $\Delta\theta(t) \approx 0$). The LO-LO BI in the case of the SSB signal is written as:

$$I^{\text{SSB}}_{\text{LO-LO BI}} \propto \frac{\text{R}}{2}|E_{\text{LO}}|^2$$

$$\propto \frac{\text{R}}{2}|A_{\text{LO}}e^{j(\varphi(t)+\theta(t))}|^2$$

$$\propto \frac{1}{2}\text{R}A^2_{\text{LO}} \quad (14)$$

As the SSB signal is only frequency/phase modulated, the LO-LO BI after photodetection is simply a constant DC component as shown in Eq. 14, which can be filtered out using a DC blocker, and thus the LO-LO BI is avoided, whether or not a guard band is used.

III. EXPERIMENTAL AND SIMULATION SETUPS

To investigate the impact of DD distortions arising from single-photodiode detection, especially the LO-LO BI, on the receiver sensitivity of a coherent LiDAR system, the setup shown in Fig. 2 was employed for both Monte Carlo simulations and experimental demonstration.

In the experiment, an optical delay line L of 385 m of standard single-mode fiber (SSMF) with an effective refractive index n of approximately 1.5 was used to emulate the time-of-flight of the signal [20], [23]. At the transmitter, an external cavity laser centered at 1551.12 nm was used, with an output power of 9.6 dBm and a linewidth of approximately 100 kHz. The laser coherence length was approximately 637 m in the SSMF, and thus the delay line was well within the coherence length [20]. The ECL was externally modulated via IQM (Oclaro 6M0C6400) driven by a digital-to-analog converter (DAC) sampling at 92 GSa/s. The
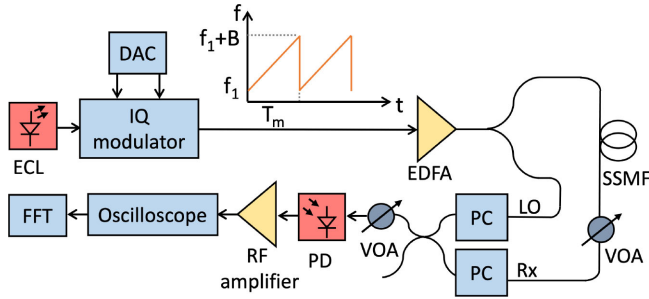
Fig. 2. System setup of single-photodiode based coherent LiDAR. ECL: external cavity laser; IQ: in-phase and quadrature; DAC: digital-to-analog converter; EDFA: Erbium-doped fiber amplifier; SSMF: standard single-mode fiber; VOA: variable optical attenuator; LO: local oscillator; Rx: received signal; PC: polarization controller; PD: photodiode; RF: radio frequency; FFT: fast Fourier transform.
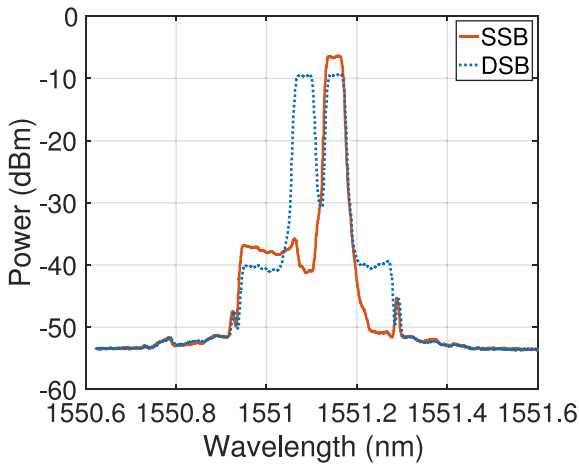

Fig. 3. Transmitted DSB and SSB signals (2 GHz guard band, 5 GHz chirp) measured by an optical spectrum analyzer at 0.01 nm resolution bandwidth.

extinction ratio of the IQM was approximately 40 dB. For the sawtooth chirp signal, the pulse period T_m was set as 5 μs and the chirping bandwidth $B = 5$ GHz. The corresponding beat frequency $f_b = \frac{LnB}{cT_m} \approx 1.92$ GHz. In order to investigate how LO-LO BI affects Rx sensitivity, two values of guard band width were assessed: 0 and 2 GHz (i.e., $f_1 = 0$ GHz and $f_1 = 2$ GHz). Eq. 6 was used to drive the IQM to generate the complex-valued SSB signal. For the DSB signal, both arms of the IQM were driven by the same waveform (Eq. 2) in order to achieve the same output power as the SSB signal. The peak-to-peak driving voltage was set to approximately 1 V_π to maximize the output power after modulation. The modulated optical signal was then amplified to 17.3 dBm by an EDFA with a noise figure of 5.5 dB. Note that, in a commercial system, a semiconductor optical amplifier (SOA) [31] or a compact micro EDFA [32], [33] could be used to reduce the cost and size.

Fig. 3 shows an example of the transmitted signal spectra (2 GHz guard band, 5 GHz chirping bandwidth) measured using an optical spectrum analyzer (OSA) at a resolution bandwidth of 0.01 nm. For both SSB and DSB signals, a noise pedestal (15 GHz) which is about 30 dB lower than the signal power is observed to the side of the desired 5 GHz chirp spectra.

This was caused by modulator nonlinearity, introducing a modulation sideband. The signal was then split by a 3-dB splitter into two paths; one for signal transmission and the other to serve as the LO at the receiver. A variable optical attenuator (VOA) was added before the receiver to adjust the Rx signal power.

At the receiver, the polarization states of the Rx signal and LO were first aligned by two polarization controllers (PCs) to maximize the beating [26], [30], and then combined with a 3-dB coupler. The LO power at the input of the 3-dB coupler was 13.4 dBm and the Rx signal power was swept from -10.6 dBm to -66.8 dBm with a step size of -5 dB. A 6-dB optical attenuator was applied before the PD to reduce the total incident optical power below its maximum input power. In order to show the full-spectrum of the signal and DD beating interference, a PD with a bandwidth of 15 GHz was used with 0.6 A/W responsivity, followed by a radio frequency (RF) amplifier with 17 dB gain. Finally, the signal was digitized by a real-time oscilloscope sampling at 50 GSa/s. At each Rx power, 100 measurements were saved to test the reliability of DSB and SSB signals, each of 25 000 sampling points (i.e., one pulse period of 5 μs). A Fourier transform was applied off-line using MATLAB. The desired beat frequency f_b was extracted by identifying the beating tone with the highest power in the frequency domain, and converted into distance through $L = \frac{f_b c T_m}{nB}$.

Monte Carlo simulations were also carried out using MATLAB, with the system structure and parameters used in the experiments as described above. The laser phase noise was modelled as a random walk, specifically the Wiener process described by [34]:

$$\theta(t) - \theta(t - \Delta t) \sim \mathcal{N}(0, 2\pi\Delta v \Delta t) \tag{15}$$

where Δt indicates a small time offset and Δv denotes the laser linewidth which was 100 kHz in simulation. $\mathcal{N}(0, 2\pi\Delta v \Delta t)$ denotes a normal distribution with zero mean and the variance of $2\pi\Delta v \Delta t$. As with the experiments, at each distance and received signal power, 100 simulations were performed.

IV. RESULTS AND DISCUSSION

In this section, we first discuss the impact of LO-LO BI on the receiver sensitivity for DSB and SSB signals through Monte Carlo simulations in Section IV.A. The simulated results are then compared to the experimental performance in Section IV.B. In Section IV.C, we further discuss the relation between the laser coherence length which is limited by the laser phase noise, and the receiver sensitivity for both DSB and SSB signals.

A. Impact of LO-LO BI via Monte Carlo Simulations

In simulation, we first employed a sufficiently wide guard band to ensure LO-LO BI terms fell at frequencies outside the desired signal band (i.e., $f_1 = 2$ GHz), and thus the system performance was limited by LO-ASE beating interference. Fig. 4 shows the simulated average power at the beat frequency versus Rx power. The vertical bar at each Rx power represents the standard deviation of the beat frequency power over 100 simulations. It can be seen that the DSB signal experiences much greater power fluctuation than the SSB signal. This is explained
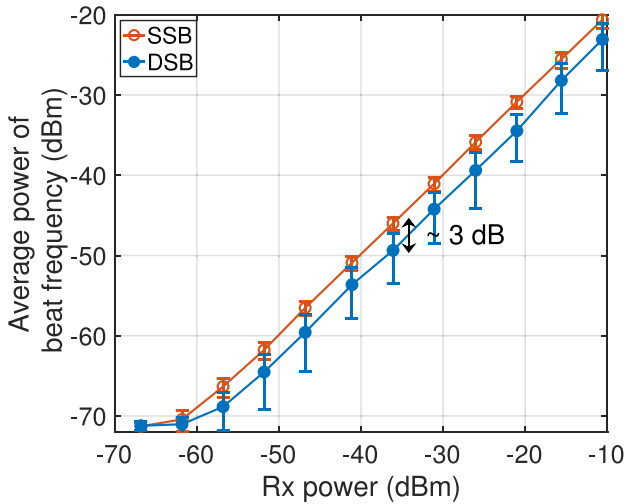
Fig. 4. Simulated average power at the beat frequency versus Rx power for DSB and SSB signals. The vertical error bars indicate the standard deviation of the beat frequency power.

by Eq. 11 which shows that for the DSB signal, the laser phase noise is converted to amplitude noise after photodetection. Such fluctuation leads to a ∼3 dB reduction of the average power of the beat frequency over 100 simulations compared to that of the SSB signal.

The power fluctuation caused by the DSB signal might not be an issue when the Rx power is sufficiently high as the desired beat frequency can still be discerned from the noise floor. Nevertheless, at low Rx powers, e.g. for targets at long-distance, the power of the beat frequency might fall below the noise floor and thus the distance estimation will not always be reliable. Fig. 5(a) shows the standard deviation of the distance estimation as a function of the Rx power obtained by the Monte Carlo simulations. The inset shows an example of frequency-domain power spectra of the detector photocurrent for DSB and SSB signals at the Rx power of −21.02 dBm in simulation. The desired beat frequency is at 1.92 GHz. The beating tone at 3.08 GHz is due to the discontinuity of the sawtooth waveform [13]. For the DSB signal, the nonlinear LO-LO BI is observed over the range from 4 to 14 GHz with twice the bandwidth of the signal's 5 GHz chirp as explained by Eq. 12, and it is approximately 25 dB higher than the LO-ASE BI limited noise floor. For the SSB signal, the LO-LO BI is simply a DC term as suggested by Eq. 14. As the DC component can be filtered out using a DC blocker in the experiment, we have subtracted the mean of detected signal waveforms in the simulation to achieve the same effect, and that is why the DC term which should be at zero frequency is not present in the frequency-domain spectra for both DSB and SSB signals. Ideally, the LO-ASE noise floor is the broad-band white noise with a constant power spectral density. However, in order to replicate the actual experimental setup, a non-ideal modulator of approximately 40 dB extinction ratio was assumed [35], and modulation nonlinearity was also included in the simulation. This limited extinction ratio of the modulator leads to a weak residual carrier beating with the signal on reception, accounting for the additional noise from 2–7 GHz (around 5 dB higher than
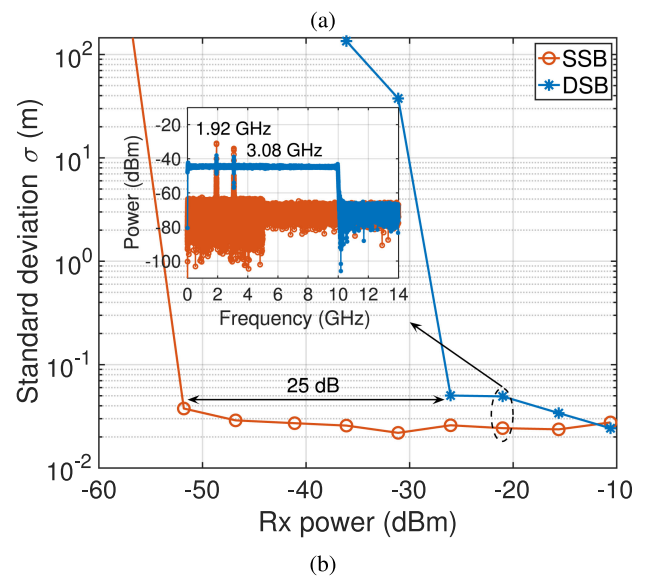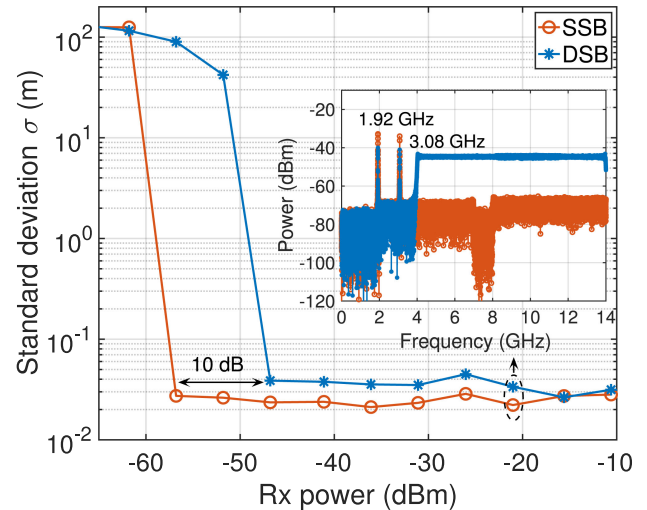

(a)

(b)

Fig. 5. Simulated standard deviation of distance estimation versus Rx power with (a) 2 GHz guard band, and (b) without guard band. The inset in each figure shows the frequency-domain spectra of SSB and DSB signals.

LO-ASE BI noise floor) with the same bandwidth as the chirp signal. The extra noise at frequencies above 8 GHz is caused by the nonlinearity of the modulator. Note that both these distortions exist in the DSB signal power spectrum but are masked by the dominant LO-LO BI in the high-frequency regime. In this case, with a sufficient guard band, the unwanted LO-LO BI is not at the same frequency range as the desired beat signal.

As shown in the plot of standard deviation versus Rx power in Fig. 5(a), at Rx powers higher than −46.8 dBm, both DSB and SSB signals can accurately predict distance, showing a standard deviation of distance estimation of approximately 0.03 m. As the Rx power decreases, for the DSB signal, the power fluctuation causes several inaccurate distance estimations over the 100 simulations and thus the standard deviation starts to increase. In contrast, the SSB signal demonstrates 10 dB better receiver sensitivity, and can operate reliably with Rx signal powers down to −56.8 dBm.
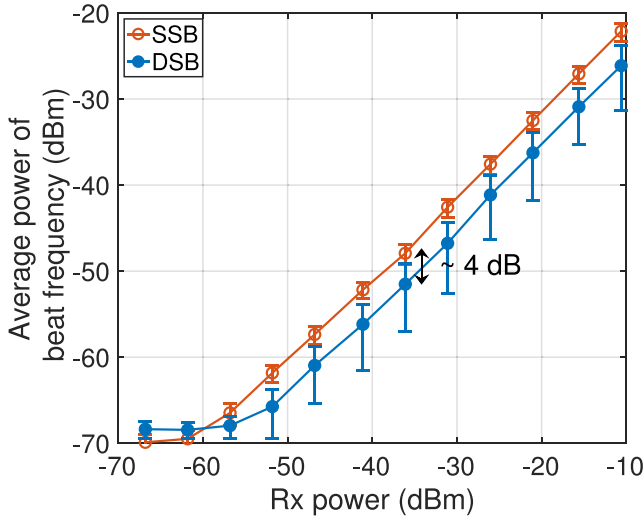
Fig. 6. Experimental average power at the beat frequency versus Rx power for DSB and SSB signals. The vertical error bars indicate the standard deviation of the beat frequency power.

To assess the impact of DD interference, the guard band was removed such that the LO-LO BI overlapped with the desired beat signal band in the frequency domain as shown in the inset of Fig. 5(b). Compared to the results with the 2 GHz guard band given in Fig. 5(a), the minimum Rx power for the SSB signal increases from -56.8 dBm to -51.8 dBm due to residual-carrier beating with the signal; a 5 dB penalty in receiver sensitivity. For the DSB signal, however, as the LO-LO BI is unmitigated, a 20 dB receiver sensitivity penalty is measured (i.e., from -46.8 dBm with a 2 GHz guard band to -26.04 dBm without a guard band). Therefore, in this case without a guard band, the SSB signal shows 25 dB better receiver sensitivity than the DSB signal.

B. Impact of LO-LO BI Via Experimental Demonstration

Experiments were also carried out and the results were compared with the simulation results. Fig. 6 shows the experimental average power at the desired beat frequency versus Rx power for DSB and SSB signals. Similar to the simulation results in Fig. 4, the DSB signal experiences a higher power fluctuation shown by the larger standard deviation at each received signal power level, which leads to a ∼4 dB reduction of the average beat signal power over 100 measurements compared to that of SSB signal. Note that at each Rx power, there is a small discrepancy in the average powers between the experimental and simulated results. This might be caused by the non-ideal polarization alignment in the experiment which was manually tuned with the polarization controller, leading to about a 2 dB reduction of the average power of the beat frequency.

Fig. 7(a) and (b) present, from the experiments, the standard deviation of the distance estimation as a function of Rx power with a 2 GHz guard band and without a guard band, respectively. The inset in each figure shows the experimental frequency-domain spectra of SSB and DSB signals at the Rx power of -21.02 dBm. Each spectrum looks similar to the simulated one
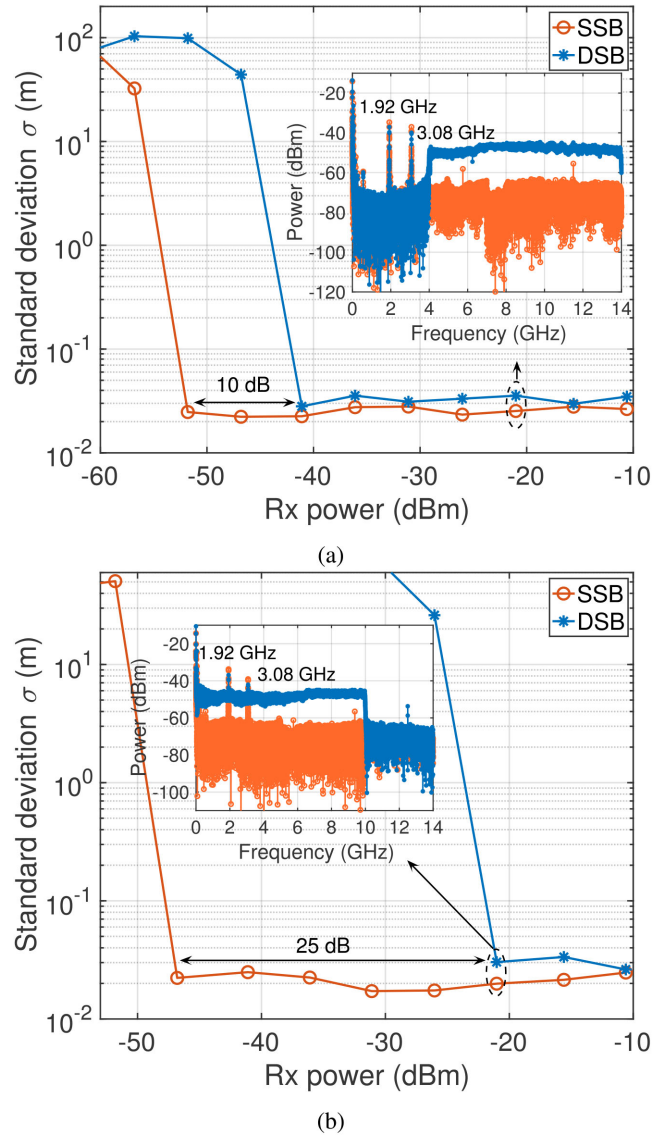

(a)

(b)

Fig. 7. Experimental standard deviation of distance estimation versus Rx power with (a) 2 GHz guard band and (b) without guard band. The inset in each figure shows the frequency-domain spectra of SSB and DSB signals.

shown in Fig. 5. Despite the main nonlinear interference such as LO-LO BI and the penalty from the non-ideal modulator which are also observed in the simulation, a few spectral components at frequencies below 600 MHz occur only in the experimental spectra for both DSB and SSB signals. As those components, which are generated by the transceiver are constant for all measurements, they can be removed through system calibration. Thus, in order to assess the limitation due to the LO-ASE beating noise floor, only frequency components between 600 MHz and 2 GHz were measured to identify the desired beat frequency.

In the case with a sufficiently wide guard band as shown in Fig. 7(a), there is a 10 dB sensitivity difference between SSB and DSB signals, the same as that observed in the simulation results shown in Fig. 5(a), and this is due to the phase noise induced power fluctuation of the DSB signal. Removing the guard band so that the LO-LO BI falls within the frequency range

of the desired beat signal as plotted in the inset of Fig. 7(b), the sensitivity difference between the DSB and SSB signals therefore increases to 25 dB. It should be noted that though the sensitivity difference between the DSB and SSB signals is the same as the simulation, the experimental results show a 5 dB worse receiver sensitivity than the simulation (e.g., with a 2 GHz guard band: the Rx sensitivity is -56.8 dBm for SSB signal in simulation and -51.8 dBm in experiment; for DSB signal: -46.8 dBm in simulation and -41.1 dBm in experiment. The same offset is observed in the case without a guard band.). In addition to the measurements with a delay line of 385 m, giving the above results, we also carried out measurements with a delay line of 238 m, and a similar performance was observed in both simulations and experiments.

C. Impact of Laser Phase Noise

We have so far discussed the penalty of DD distortions specifically the LO-LO BI through both numerical and experimental results. For the DSB signal, when the LO-LO BI is mitigated through the use of a spectral guard band, its receiver sensitivity is still affected by laser phase noise induced power fluctuation as suggested by Eq. 11 even within the laser coherence length. Such power fluctuation leads to a 10 dB receiver sensitivity penalty at a delay length of 385 m compared to that observed with the SSB signal as shown in Fig. 5(a) and Fig. 7(a). It is also indicated by Eq. 11 that, the shorter the delay line is, the more coherent is the laser phase noise between the LO and Rx signal. As phase noise is converted to amplitude noise after photodetection, a higher power fluctuation and thus a worse receiver sensitivity would be expected at a shorter delay length, making the DSB signal less reliable. In contrast, for the SSB signal as suggested by Eq. 13, reducing the delay results in the relative phase noise between the LO and Rx signal approaching zero. In the frequency domain, the spectral broadening due to laser phase noise therefore will be smaller, and the majority of the desired beat signal power will be centered around a single beat frequency leading to a more accurate distance estimation.

In order to evaluate how such phase noise coherence affects the receiver sensitivity of DSB and SSB signals, we therefore conducted more experiments, decreasing the delay line to 238 m, 132 m, 63 m and 44 m. All the measurements were performed with 5 GHz chirping bandwidth and 2 GHz guard band mitigating the penalty from LO-LO BI, so the system performance was limited by the LO-ASE beating noise floor. Extensive Monte Carlo simulations were also carried out with the delay line varying from 20 m to 395 m. The maximum beat frequency at 395 m is 1.975 GHz, which is still within the 2 GHz guard band ensuring the LO-LO BI will not interfere with the desired beat signal. The received signal power was varied from -10.6 dBm, decreased in steps of 2 dB down to -66.6 dBm.

The receiver sensitivity difference between DSB and SSB signals with varying delay length is shown in Fig. 8. The simulation results show that at a shorter delay length, for example, at 20 m, there is a 40 dB sensitivity difference between DSB and SSB signals. As the delay increases, the sensitivity difference decreases and levels out at around 10 dB with distances above
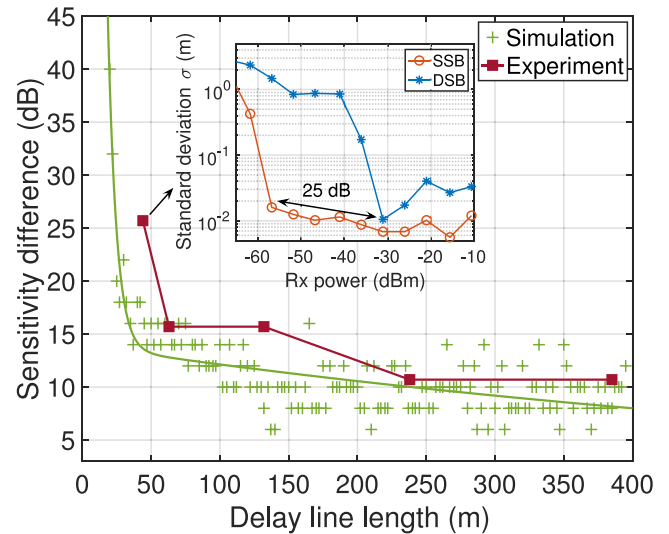

Fig. 8. Receiver sensitivity difference between DSB and SSB signals versus delay line length. The green solid line is the nonlinear fitted curve of the simulation results. The inset shows the experimental standard deviation of distance estimation versus Rx power at the delay line length of 44 m.

100 m. The experimental results show a similar trend with a higher sensitivity difference between DSB and SSB signals at shorter delay distances. For example, the inset of Fig. 8 plots the standard deviation of distance estimation versus received signal power at a delay line length of 44 m and the result indicates a 25 dB sensitivity difference. Increasing the delay, the sensitivity difference gradually flattens out to approximately 10 dB at delay line distances of 238 m and 385 m. The reason for this larger sensitivity difference at a shorter delay distance is two-fold. On the one hand, the SSB signal achieves a better sensitivity at shorter distances as the phase noise variation becomes negligible, e.g., -56.8 dBm at 44 m and -51.8 dBm at 385 m (see Fig. 7(a)). On the other hand, the beating signal power fluctuation with the DSB signal is larger due to the increased coherence of the phase noise between LO and Rx signal, and thus the required Rx power increases from -41.1 dBm at 385 m (see Fig. 7(a)) to -31.1 dBm at 44 m. The results may suggest that with reducing distance to the target, the DSB signal requires increasing Rx power to allow the desired beat tone to be identified. In practice for a LiDAR system, the received signal after being reflected from a close target usually has a higher power than one reflected from a more distant target, and therefore, such power fluctuation of the DSB signal might not be a major issue.

It should noted that the above results were obtained using an optical fiber delay line to emulate the time-of-flight; it is necessary to carry out free-space demonstrations in the future as the interference from the surrounding environment may degrade the quality of the received signal. Nevertheless, as the LO-LO BI is only related to the LO not to the received signal, it will always be present in this single-photodiode based coherent LiDAR configuration regardless of the interference from free-space. Therefore, compared to the DSB signal, the receiver sensitivity benefit offered by the SSB signal would still be expected in free-space operation.

The single-photodiode based coherent LiDAR receiver as discussed in this paper is low-cost and low-complexity compared to a balanced phase-diversity coherent receiver; however, its sensitivity is limited by the LO-ASE beating noise floor (DD distortion) when LO-LO BI is mitigated. For comparison, we have carried out experiments using a balanced phase-diversity coherent receiver with the same signals (SSB and DSB signals with 2 GHz guard band and 5 GHz chirp) and delay line length of 385 m. This system has approximately 15 dB better sensitivity than the single photodiode-based coherent receiver. This is due to the mitigation of LO-ASE beating interference through balanced detection and, in the case of DSB signals, the avoidance of phase noise to amplitude noise conversion. Nonetheless, for the DSB signal without a guard band, the balanced phase-diversity coherent receiver performance is susceptible to the finite common mode rejection ratio as the LO-LO BI is only partially mitigated. The impact of finite common mode rejection ratio on the sensitivity of balanced receivers (both 3-dB coupler-based and phase-diversity optical hybrid-based receivers) in coherent LiDAR will be the subject of future research.

V. CONCLUSION

We evaluated the performance of two linear frequency-modulated chirp signals: the frequency-modulated continuous-wave SSB signal and the amplitude-modulated DSB signal in coherent LiDAR systems with single-photodiode detection. We analyzed the impact of direct-detection beating distortions especially LO-LO beating interference on the receiver sensitivity through both simulations and experiments. The results indicate that the DSB signal suffers a significant receiver sensitivity penalty from nonlinear LO-LO BI; a 20 dB receiver sensitivity penalty is observed at a delay line length of 385 m. Therefore, in order to work at low received signal power, the DSB signal requires a sufficiently wide spectral guard band to mitigate LO-LO BI, achieved at the expense of requiring a larger electrical bandwidth. Furthermore, the DSB signal is susceptible to power fluctuation caused by laser phase noise after photodetection, making it less reliable especially at shorter distances.

These two main drawbacks associated with the DSB signal can be overcome through the use of a complex-valued SSB FMCW signal at the expense of using a more complex IQ modulator at the transmitter. The LO-LO BI is not problematic when using a SSB signal since it is just a DC component which can be easily filtered out. Thus, for a SSB signal, a guard band is not necessary and the entire electrical bandwidth can be utilized for the chirp signal to achieve a better resolution. In both simulations and experiments, with a frequency chirp bandwidth of 5 GHz, and with no guard band, it is shown to outperform the DSB signal-based system with 25 dB better receiver sensitivity with a 385 m delay line length. In addition, the use of a SSB signal with the single-photodiode based coherent receiver makes it more tolerant to laser phase noise, as it does not suffer from phase noise to amplitude noise conversion, as experienced with the DSB signal. In particular, the impact of laser phase noise is negligible when operating within the laser coherence length. Particularly at a shorter delay line length of 44 m, the use of a

SSB signal significantly relaxes the requirement for the received signal power; at this distance, it offers a 25 dB sensitivity advantage, even when the LO-LO BI is mitigated in the DSB signal-based system by a spectral guard band.

REFERENCES

[1] X. Mao, D. Inoue, S. Kato, and M. Kagami, "Amplitude-modulated laser radar for range and speed measurement in car applications," *IEEE Trans. Intell. Transp. Syst.*, vol. 13, no. 1, pp. 408–413, Mar. 2012.

[2] D. J. Lum, S. H. Knarr, and J. C. Howell, "Frequency-modulated continuous-wave LiDAR compressive depth-mapping," *Opt. Exp.*, vol. 26, no. 12, pp. 15 420–15 435, 2018.

[3] P. Feneyrou *et al.*, "Frequency-modulated multifunction lidar for anemometry, range finding, and velocimetry-1. theory and signal processing," *Appl. Opt.*, vol. 56, no. 35, pp. 9663–9675, 2017.

[4] C. F. Abari, A. T. Pedersen, and J. Mann, "An all-fiber image-reject homodyne coherent Doppler wind lidar," *Opt. Exp.*, vol. 22, no. 21, pp. 25 880–25 894, 2014.

[5] B. Behroozpour *et al.*, "Electronic-photonic integrated circuit for 3D microimaging," *IEEE J. Solid-State Circuits*, vol. 52, no. 1, pp. 161–172, Jan. 2017.

[6] D. Onori, F. Scotti, M. Scaffardi, A. Bogoni, and F. Laghezza, "Coherent interferometric dual-frequency laser radar for precise range/Doppler measurement," *J. Lightw. Technol.*, vol. 34, no. 20, pp. 4828–4834, 2016.

[7] C. Allen, Y. Cobanoglu, S. K. Chong, and S. Gogineni, "Performance of a 1319 Nm laser radar using RF pulse compression," in *Proc. Int. Geosci. Remote Sens. Symp.*, 2001, pp. 997–999.

[8] P. Adany, C. Allen, and R. Hui, "Chirped lidar using simplified homodyne detection," *J. Lightw. Technol.*, vol. 27, no. 16, pp. 3351–3357, 2009.

[9] A. Martin *et al.*, "Photonic integrated circuit-based FMCW coherent LiDAR," *J. Lightw. Technol.*, vol. 36, no. 19, pp. 4640–4645, 2018.

[10] C. V. Poulton *et al.*, "Coherent solid-state LIDAR with silicon photonic optical phased arrays," *Opt. Lett.*, vol. 42, no. 20, pp. 4091–4094, 2017.

[11] E. W. Mitchell *et al.*, "Coherent laser ranging for precision imaging through flames," *Optica*, vol. 5, no. 8, pp. 988–995, 2018.

[12] E. Baumann, F. R. Giorgetta, J.-D. Deschênes, W. C. Swann, I. Coddington, and N. R. Newbury, "Comb-calibrated laser ranging for three-dimensional surface profiling with micrometer-level precision at a distance," *Opt. Exp.*, vol. 22, no. 21, pp. 24 914–24 928, 2014.

[13] D. Uttam and B. Culshaw, "Precision time domain reflectometry in optical fiber systems using a frequency modulated continuous wave ranging technique," *J. Lightw. Technol.*, vol. 3, no. 5, pp. 971–977, 1985.

[14] S. Kakuma, "Frequency-modulated continuous-wave laser radar using dual vertical-cavity surface-emitting laser diodes for real-time measurements of distance and radial velocity," *Opt. Rev.*, vol. 24, no. 1, pp. 39–46, 2017.

[15] C. J. Karlsson, F. Å. Olsson, D. Letalick, and M. Harris, "All-fiber multifunction continuous-wave coherent laser radar at 1.55 μm for range, speed, vibration, and wind measurements," *Appl. Opt.*, vol. 39, no. 21, pp. 3716–3726, 2000.

[16] X. Zhang, J. Pouls, and M. C. Wu, "Laser frequency sweep linearization by iterative learning pre-distortion for FMCW LiDAR," *Opt. Exp.*, vol. 27, no. 7, pp. 9965–9974, 2019.

[17] M.-C. Amann, T. M. Bosch, M. Lescure, R. Myllylä, and M. Rioux, "Laser ranging: A critical review of unusual techniques for distance measurement," *Opt. Eng.*, vol. 40, no. 1, pp. 10–19, 2001.

[18] N. Satyan, A. Vasilyev, G. Rakuljic, V. Leyva, and A. Yariv, "Precise control of broadband frequency chirps using optoelectronic feedback," *Opt. Exp.*, vol. 17, no. 18, pp. 15 991–15 999, 2009.

[19] B. Behroozpour, P. A. Sandborn, M. C. Wu, and B. E. Boser, "Lidar system architectures and circuits," *IEEE Commun. Mag.*, vol. 55, no. 10, pp. 135–142, Oct. 2017.

[20] T. Kim, P. Bhargava, and V. Stojanović, "Overcoming the coherence distance barrier in long-range FMCW LIDAR," in *Proc. Conf. Lasers Electro-Opt.*, p. STh3L.7, 2018, pp. 1–2.

[21] N. Kobayashi *et al.*, "Silicon photonic hybrid ring-filter external cavity wavelength tunable lasers," *J. Lightw. Technol.*, vol. 33, no. 6, pp. 1241–1246, 2015.

[22] C. G. H. Roeloffzen *et al.*, "Low-loss Si_3N_4 triplex optical waveguides: Technology and applications overview," *IEEE J. Sel. Top. Quantum Electron.*, vol. 24, no. 4, pp. 1–21, 2018.

[23] S. Gao and R. Hui, "Frequency-modulated continuous-wave lidar using i/q modulator for simplified heterodyne detection," *Opt. Lett.*, vol. 37, no. 11, pp. 2022–2024, 2012.

[24] Z. Xu, H. Zhang, K. Chen, D. Zhu, and S. Pan, "FMCW lidar using phase-diversity coherent detection to avoid signal aliasing," *IEEE Photon. Technol. Lett.*, vol. 31, no. 22, pp. 1822–1825, Nov. 2019.

[25] S. Gao, M. O'Sullivan, and R. Hui, "Complex-optical-field lidar system for range and vector velocity measurement," *Opt. Exp.*, vol. 20, no. 23, pp. 25 867–25 875, 2012.

[26] Z. Xu, L. Tang, H. Zhang, and S. Pan, "Simultaneous real-time ranging and velocimetry via a dual-sideband chirped lidar," *IEEE Photon. Technol. Lett.*, vol. 29, no. 24, pp. 2254–2257, 2017.

[27] P. A. Sandborn, N. Kaneda, Y.-K. Chen, and M. C. Wu, "Dual-sideband linear FMCW lidar with homodyne detection for application in 3D imaging," in *Proc. Conf. Lasers Electro-Opt.*, 2016, pp. 1–2

[28] T. Liao, M. Hameed, and R. Hui, "Bandwidth efficient coherent lidar based on phase-diversity detection," *Appl. Opt.*, vol. 54, no. 11, pp. 3157–3161, 2015.

[29] M. Seimetz, *High-Order Modulation for Optical Fiber Transmission*. Berlin, Germany: Springer, 2009.

[30] B. La Lone, B. Marshall, E. Miller, G. Stevens, W. Turley, and L. Veeser, "Simultaneous broadband laser ranging and photonic doppler velocimetry for dynamic compression experiments," *Rev. Sci. Instrum.*, vol. 86, no. 2, p. 0 23112, 2015 Art. no. 023112.

[31] Accessed on: May 2021. [Online]. Available: https://www.neophotonics.com/products/semiconductor-optical-amplifier-soa/

[32] Accessed on: May 2021. [Online]. Available: https://ii-vi.com/product/flexsom-edfa/

[33] Accessed on: May 2021. [Online]. Available: https://www.epsglobal.com/Media-Library/EPSGlobal/Products/files/finisar/roadm-fws-optoelectronic/Single-Channel-Micro-EDFA.pdf?ext=.pdf

[34] M. G. Taylor, "Phase estimation methods for optical coherent detection using digital signal processing," *J. Lightw. Technol.*, vol. 27, no. 7, pp. 901–914, 2009.

[35] Accessed on: May 2021. [Online]. Available: https://www.lasercomponents.com/de/?embedded=1&file=fileadmin/user_upload/home/Datasheets/ixblue/mxiqer-ln-30.pdf&no_cache=1